Synthesis

Mater. Res. Soc. Symp. Proc. Vol. 1174 © 2009 Materials Research Society 1174-V09-31

Fabrication of Nano-Sized Tin Oxide Powder by Spray Pyrolysis Process

Jaekeun Yu, Jwayeon Kim and Jeoungsu Han

Department of Advanced Materials Engineering, Hoseo University, Asan 336-795, Korea

ABSTRACT

By using tin chloride solution as the raw material, a nano-sized tin oxide powder with average particle size below 50 nm is generated by spray pyrolysis reaction. This study also examines the influences of the reaction parameters such as reaction temperature and the concentration of raw material solution on the powder properties. As the reaction temperature increases from 800 to 850 ℃, the average particle size of the generated powder increases from 20 nm to 30 nm. As the reaction temperature reaches 900 ℃, the droplets are composed of nano-particles with average size of 30 nm, while the average size of individual particles increases remarkably up to 80~100 nm. When the tin concentration reaches 75 g/L, the average particle size of the powder is below 20 nm. When the tin concentration reaches 150 g/L, the droplets are composed of nano particles with average size around 30 nm, whereas the average size of independent particles increases up to 80~100 nm. When the concentration reaches 400 g/L, the droplets are composed of nano-particles with average size of 30 nm.

INTRODUCTION

Spray pyrolysis reaction[1-7] is the method of manufacturing nano-sized metal oxide powder. In this reaction, chemical components are uniformly blended in the solution state so as to make a complex solution, which is in turn sprayed into a reaction furnace with a high temperature. In the furnace, spray pyrolysis reaction is accomplished instantly, and as a result, the ultra-fine metal oxide powder is formed. The purpose of this study is to develop a technology for the mass production of nano-sized tin oxide powder with uniform particle size and average particle size below 50 nm in a spray pyrolysis reaction device by using tin chloride solution as the raw material. This study also examines the influences of reaction parameters on the properties of the generated tin oxide powder. These parameters include the reaction temperature and the concentration of raw material solution.

EXPERIMENT

In this study, a tin oxide powder with average particle size below 50 nm is manufactured from the tin chloride solution with the presence of tetravalent tin ions by using spray pyrolysis process. First, tin powder with purity above 99.9 % is dissolved into the hydrochloric acid

solution with concentration of 25 % until the concentration of tin constituent is adjusted to 400 g/L. A certain amount of ammonia is added in the solution so as to oxidize all the divalent tin ions into tetravalent ones. Then, the solution is filtered triply through filter paper, and the purified solution is utilized as the raw material of the spray pyrolysis process. The constituents of silicon dioxide, phosphorus, calcium, chromium and copper in this solution are below 100 ppm. This solution is diluted by distilled water so that the tin concentration of the solution is respectively adjusted to 400, 300, 150 and 75 g/L.

In order to generate the nano-sized tin oxide powder, a spray pyrolysis system is specially designed and built for this study. The schematic diagram of this system is shown in Figure 1. The properties of the generated powder are examined according to TEM analysis (the generation of single crystal particles), SEM analysis (particle size distribution and particle shape), and XRD analysis (powder phase and composition).

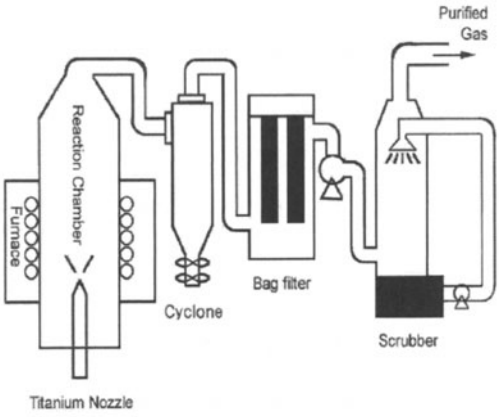

Figure 1. Schematic diagram of spray pyrolysis system

DISCUSSION

The Powder properties influenced by the reaction temperature

Figure 2 is the 30,000 times magnified image under SEM, which shows the property change of the generated powder relative to the rise of reaction temperature from 800 ℃ to 950 ℃. Figure 3 is the 200,000 times magnified image under SEM, which shows the property change of the generated powder under the same reaction conditions as of Figure 2.

When the reaction temperature is at 800 ℃ as shown in Figure 2 (a), the generated powder maintains the spherical shape of droplets micronized at the initial stage of pyrolysis reaction, the particle size is larger than those at the other reaction temperatures, and the particle size distribution appears to be comparatively uniform. According to the result shown in Figure 3 (a), it can be concluded that the droplets shown in Figure 2 (a) are composed of nano-sized particles with average particle size around 20 nm. When the reaction temperature increases up to 900 ℃,

there are extremely severe bursts of droplets at the initial stage of pyrolysis reaction. According to the result shown in Figure 3 (c), the droplets shown in Figure 2 (c) consist of nano-sized particles with average particle size around 30 nm, while the particles are combined much more compactly in contrast to the case at 850 ℃. For the independent particles, however, the average particle size remarkably increases up to 80~100 nm, and the particle surface becomes comparatively compact. When the reaction temperature increases up to 950 ℃, there is a much severer burst of droplets at the initial stage of pyrolysis reaction in contrast to the case at 900 ℃. As shown in Figure 2 (d), among all the powder generated by pyrolysis reaction, the ratio of the powder that maintains the spherical shape of droplets micronized at the initial stage decreases sharp, and the majority of the generated powder are in the shape of independent particles.

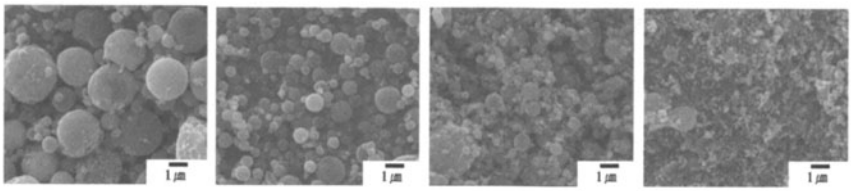

(a) 800 °C (b) 850 °C (c) 900 °C (d) 950 °C

Figure 2. SEM photographs of produced powder according to various reaction temperatures at raw material solution of 150 g/ℓ Sn, 20 mL/min. inlet speed of solution, 2 mm nozzle tip size and 3 kg/cm^2 air pressure. (X 30,000)

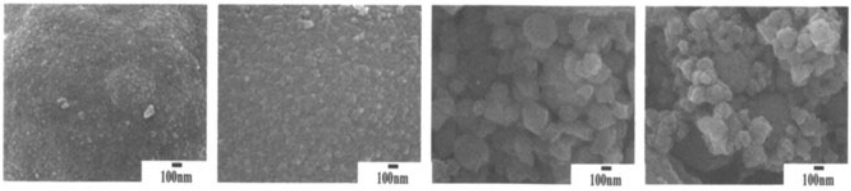

(a) 800 °C (b) 850 °C (c) 900 °C (d) 950 °C

Figure 3. SEM photographs of produced powder according to various reaction temperatures at raw material solution of 150 g/ℓ Sn, 20 mL/min. inlet speed of solution, 2 mm nozzle tip size and 3 kg/cm^2 air pressure. (X 200,000)

Figure 4 is the result of TEM analysis, (a) which shows the structural property of the generated powder, and (b)the diffraction pattern of one particle for identifying the single crystal of oxide particles. Because other particles have the similar patterns, the compact single crystal structure of the generated powder can be confirmed by this analysis.

(a) TEM photographs of produced powder. (b) Selective diffraction pattern of single particle.

Figure 4. TEM photographs of produced powder and selective diffraction pattern(zone axis [$\bar{1}$10]) of single particle at reaction temperature of 900℃, raw material solution of 150g/L tin, 20 mL/min. inlet speed of solution, 2 mm nozzle tip size and 3 kg/cm^2 air pressure.

Fig. 5 is the results of XRD analysis under the same reaction conditions as shown in Fig. 2. As the reaction temperature increases from 800 to 900℃, the intensities of the first, second and third peaks greatly increases, resulting the combined effect of the following facts: a) the average particle size of independent single crystals increases remarkably; and b) the single crystals inside the particles, which are in the shape of droplet, are much compactly combined together. When the reaction temperature increases ups to 950℃, the overall peak intensity decreases greatly, resulting the fact: at the temperature of 950℃, the ratio of the droplet types, in which tin oxide single crystals aggregate, decreases sharply; and the average particle size of single crystals is smaller in contrast to the case at 900℃.

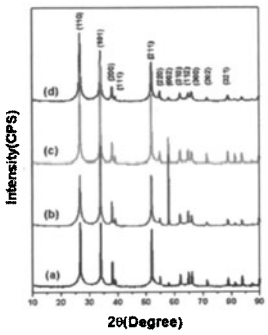

Figure 5. XRD patterns of produced powder according to reaction temperature at raw material solution of 150g/ℓ Sn, 20 mL/min. inlet speed of solution, 2 mm nozzle tip size and 3 kg/cm^2 air pressure. (a) 800°C (b) 850°C (c) 900°C (d) 950°C

The powder properties influenced by concentration of the raw material solution

Figure 6 and Figure 7 are the 30,000 and 200,000 times magnified images under SEM shown the property change of the generated powder relative to the concentration of raw material solution rising from 75 g/L to 400 g/L, respectively. When the tin concentration of raw material

solution is at the lowest 75 g/L, there is no significant difference of concentration between the surface and the center of droplet till the evaporation of solvent inside droplet ends completely. As a result, there is no severe burst of droplets during the pyrolysis reaction process. As shown in Figure 6 (a), there are two coexisting shapes among the powder generated by pyrolysis reaction such as droplets micronized at the initial stage of pyrolysis reaction and independent particles. According to Figure 7 (a), the droplets shown in Figure 6 (a) are composed of extremely small particles with average particle size below 20 nm. When the tin concentration increases up to 150 g/L, the droplet size increases remarkably contrast to the case at 75 g/L. The droplets eventually burst and the particle size distribution becomes more irregular. As shown in Figure 6 (b), the generated powder maintains the spherical shape of droplets micronized at the initial stage of pyrolysis reaction in spite of the severe burst of droplets, and the average particle size increases greatly. Moreover, the ratio of droplet-shaped particles to independent particles decreases remarkably.

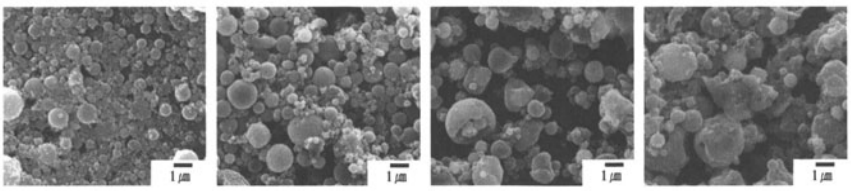

(a) 75 g/L (b) 150 g/L (c) 300 g/L (d) 400 g/L

Figure 6. SEM photographs of produced powder according to various tin concentration of raw material solution at 900℃, 20 mL/min. inlet speed of solution, 2 mm nozzle tip size and 3 kg/cm^2 air pressure. (X 30,000)

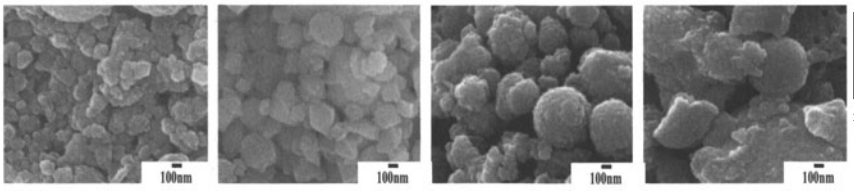

(a) 75 g/L (b) 150 g/L (c) 300 g/L (d) 400 g/L

Figure 7. SEM photographs of produced powder according to various tin concentration of raw material solution at 900℃, 20 mL/min. inlet speed of solution, 2 mm nozzle tip size and 3 kg/cm^2 air pressure. (X 200,000)

According to Figure 7 (b), the droplets shown in Figure 6 (b) consist of nano-sized particles with average particle size around 30 nm, and are rather more compactly combined together in contrast to the case at 75 g/L. For the case of independent particles, the average particle size increases to a significant level of 80~100 nm, and the particle surface becomes comparatively compact. When the concentration increases up to 400 g/L, which is close to the saturated concentration. Because the solute is excessively saturated on the droplet surface at the initial

stage of pyrolysis reaction, the decrease of droplet size caused by the evaporation of solvent is almost undetectable, and the droplet size increases greatly in contrast to the cases at low concentrations. However, because of the severe droplet burst during the pyrolysis process, the particle size distribution appears extremely irregular and the particle surface also appears in the extremely inhomogeneous shape. Also, the evaporation of solvent completes extremely fast and the evaporation heat of solvent decreases greatly during the pyrolysis process. As a result, the sintering reaction proceeds further and the droplets combine mutually each others. According to Figure 7 (d), the droplets shown in Figure 6 (d) consist of nano-sized particles with average particle size around 30 nm, and are rather compactly combined together. This result is due to the combined effect of the following two mechanisms: a) the droplet size increases with the rise of concentration after the evaporation of solvent; and b) the burst of droplets becomes severer with the rise of concentration during the pyrolysis reaction.

CONCLUSIONS

As the reaction temperature increases from 800 to 850 ℃, the average particle size of the generated powder increases from 20 nm to 30 nm, and most of the powder is in the shape of droplet. As the reaction temperature reaches 900 ℃, the droplet-shaped particles are composed of nano-particles with average size of 30 nm, while the average size of individual particles increases remarkably up to 80~100 nm. As the reaction temperature reaches 950 ℃, most of the particles appear mutually independent, while the average particle size is around 80 nm.

For the raw material solution with concentration of 75 g/L, the average particle size of the generated powder is below 20 nm, and there is a strong tendency of cohesion between particles. When the tin concentration reaches 150 g/L, the droplets are composed of nano particles with average size around 30 nm, whereas the average size of independent particles increases remarkably up to 80~100 nm. When the concentration reaches 400 g/L, the droplets are composed of nano-particles with average size of 30nm, and most of the droplets are compactly combined together.

ACKNOWLEDGMENTS

This work was supported by the Regional Innovation Center of Hoseo University in Korea.

REFERENCES

1. J.K. Yu, S.G. Kang, K.C. Chung. J.S. Han and D.H. Kim, Mater. Trans. **48**, 249 (2007).
2. J.K. Yu, S.G. Kang, J.B. Kim, J.Y. Kim, J.S. Han, J.W. Yoo, S.W. Lee and Z.S.Ahn, Mater. Trans. **47,** 1695 (2006).
3. J.K. Yu, G.H Kim, T.S. Kim and J.Y. Kim, Mater. Trans. **46,** 1695 (2005).
4. T.G. Carreno, M.P. Morales and C.J. Serna, Mater. Lett. **43,** 97 (2000),
5. D. Majumdar, T.A. Shefelbine and T.T. Kodas, J. Mater. Res. **11,** 2861 (1996).
6. M.A.A. Elmasry, A. Gaber and E.M.H. Khater, Powder Technology **90,** 165 (1997).
7. S.C. Zhang and G.L. Messing, J. Am. Ceram. Soc. **73,** 61 (1990).

Mater. Res. Soc. Symp. Proc. Vol. 1174 © 2009 Materials Research Society 1174-V03-06

Synthesis and Characterization of Nanocarbon-Supported Titanium Dioxide

Marcus A. Worsley, Joshua D. Kuntz, Octavio Cervantes, T. Yong-Jin Han, Peter J. Pauzauskie, Joe H. Satcher, Jr. and Theodore F. Baumann
Physical and Life Sciences Directorate, Lawrence Livermore National Laboratory, 7000 East Avenue, Livermore, CA 94550, U.S.A.

ABSTRACT

In this report, we describe recent efforts in fabricating new nanocarbon-supported titanium dioxide structures that exhibit high surface area and improved electrical conductivity. Nanocarbons consisting of single-walled carbon nanotubes and carbon aerogel nanoparticles were used to support titanium dioxide particles and produce monoliths with densities as low as 80 mg/cm^3. The electrical conductivity of the nanocarbon-supported titanium dioxide was dictated by the conductivity of the nanocarbon support while the pore structure was dominated by the titanium dioxide aerogel particles. The conductivity of the monoliths presented here was 72 S/m and the surface area was 203 m^2/g.

INTRODUCTION

Titanium dioxide is a widely researched material with applications ranging from photocatalysts to electrodes to hydrogen storage materials [*1-9*]. However, issues such as absorption limited to the ultraviolet range, high rates of electron-hole recombination, and relatively low surface areas have limited commercial use of titanium dioxide. Recent efforts have focused on combining titanium dioxide with various materials to address some of these issues [*8-24*]. Titanium dioxide in the presence of carbon (e.g. carbon nanotubes (CNT)) is currently one of the most attractive combinations [*13-25*]. While recent work has shown some improvements, surfaces areas and photocatalytic activity are still limited. Maintaining high surface areas while improving electrical conductivities, one could envision charging-discharging rates and photoefficiencies that are significantly higher than currently possible. Unfortunately for CNT composites, improvements in electrical conductivity are often not fully realized due to poor dispersion of CNTs in the matrix material, impeding the formation of a conductive network. However, with a mechanically robust, electrically conductive CNT foam, one could imagine simply coating this low-density CNT scaffold with titanium dioxide, yielding conductive nanocarbon-supported titanium dioxide.

Here we present the synthesis and characterization of such a high-surface area, conductive TiO_2/CNT composite. We recently reported the synthesis of a novel CNT-based foam, consisting of bundles of single-walled nanotubes (SWNT) crosslinked by carbon aerogel (CA) nanoparticles, which would serve as an excellent candidate for the CNT scaffold of the TiO_2/CNT composite. The SWNT-CA foams simultaneously exhibited increased stiffness, and high electrical conductivity even at densities approaching 10 mg cm^{-3} without reinforcement [*25*]. The foams are stable to temperatures approaching 1000°C and have been shown to be unaltered by exposure to extremely low temperatures during immersion in cryogenic liquids [*26*]. So, in addition to their use in applications such as catalyst supports, sensors, and electrodes, these ultralight, robust foams could allow the formation of novel CNT composites. As the conductive network is already established, it can be impregnated through the wicking

process [*27*] with a matrix of choice, ranging from inorganic sols to polymer melts to ceramic pastes. Thus, a variety of conductive CNT composites could be created using the SWNT-CA foam as a pre-made CNT scaffold. In this report, we use the SWNT-CA as a scaffold for the synthesis of conductive, high surface area TiO_2/CNT composites.

EXPERIMENT

Materials. All reagents were used without further purification. Resorcinol (99%) and formaldehyde (37% in water) were purchased from Aldrich Chemical Co. Sodium carbonate (anhydrous) was purchased from J.T. Baker Chemical Co. Highly purified SWNTs were purchased from Carbon Solutions, Inc.

SWNT-CA preparation. The SWNT-CAs were prepared as described in previous work [*25*]. Briefly, in a typical reaction, purified SWNTs (Carbon Solutions, Inc.) were suspended in deionized water and thoroughly dispersed using a VWR Scientific Model 75T Aquasonic (sonic power ~ 90 W, frequency ~ 40 kHz). The concentration of SWNTs in the reaction mixture was 0.7 wt%. Once the SWNTs were dispersed, resorcinol (1.235 g, 11.2 mmol), formaldehyde (1.791 g, 22.1 mmol) and sodium carbonate catalyst (5.95 mg, 0.056 mmol) were added to the reaction solution. The resorcinol to catalyst ratios (R/C) employed was 200. The amount of resorcinol and formaldehyde (RF solids) used was 4 wt%. The sol-gel mixture was then transferred to glass molds, sealed and cured in an oven at 85°C for 72 h. The resulting gels were then removed from the molds and washed with acetone for 72 h to remove all the water from the pores of the gel network. The wet gels were subsequently dried with supercritical CO_2 and pyrolyzed at 1050°C under a N_2 atmosphere for 3 h. The SWNT-CAs materials were isolated as black cylindrical monoliths. Foams with SWNT loadings of 30 wt% (0.5 vol%) were prepared by this method.

TiO_2/SWNT-CA composite preparation. Sol-gel chemistry was used to deposit the TiO_2 aerogel layer on the inner surfaces of the SWNT-CA support. The TiO_2 sol-gel solution was prepared as described in previous work [*28*]. In a typical synthesis, SWNT-CA parts were immersed in the TiO_2 sol-gel solution and full infiltration of the SWNT-CA pore network by the sol-gel solution was achieved under vacuum. Following gelation of the titania network, the wet composite was dried using supercritical CO_2, yielding the TiO_2/SWNT-CA composite.

Characterization. Bulk densities of the TiO_2/SWNT-CA composites were determined from the physical dimensions and mass of each sample. The volume percent of SWNT in each sample was calculated from the initial mass of SWNTs added, assuming a CNT density of 1.3 g/cm^3, and the final volume of the aerogel. Scanning electron microscopy (SEM) characterization was performed on a JEOL 7401-F at 10 keV (20mA) in SEI mode with a working distance of 2 mm. Transmission electron microscopy (TEM) characterization was performed on a JEOL JEM-200CX. Thermogravimetric analysis (TGA) was performed on a Shimadzu TGA 50 Thermogravimetric Analyzer to determine TiO_2 content. Samples were heated in flowing air at 10 sccm to 1000°C at 10°C/min in alumina boats. The weight fraction of material remaining was assumed to be pure stoichiometric TiO_2. Energy dispersive spectroscopy confirmed that only TiO_2 remained after TGA was performed. Surface area determination and pore volume and size analysis were performed by Brunauer-Emmett-Teller (BET) and Barrett-Joyner-Halenda (BJH) methods using an ASAP 2000 Surface Area Analyzer (Micromeritics Instrument Corporation) [*29*]. Samples of approximately 0.1 g were heated to 300°C under